

**C.P. No. 403**

(19,997)

A.R.C. Technical Report

LIBRARY  
ROYAL AIRCRAFT ESTABLISHMENT  
BEDFORD.

**C.P. No. 403**

(19,997)

A.R.C. Technical Report



MINISTRY OF SUPPLY

AERONAUTICAL RESEARCH COUNCIL

CURRENT PAPERS

**Real Gas Effects on  
Shock-Tube Performance at  
High Shock Strengths**

by

J. L. Stollery

LONDON: HER MAJESTY'S STATIONERY OFFICE

1958

PRICE 3s. 6d. NET



U.D.C. No. 533.6.011.55 : 533.6.071

Technical Note No. Aero 2413

November, 1957

ROYAL AIRCRAFT ESTABLISHMENTReal gas effects on shock-tube performance  
at high shock strengths

by

J. L. Stollery\*

SUMMARY

Calculations have been made to find the flow conditions behind shock waves in argon-free air of strengths  $M_S = U/a_1$  up to about 35. The tables used are based on the currently accepted value for the dissociation energy of nitrogen of 9.758 e.v. per molecule, and are for equilibrium conditions.

Two cases only have been considered, namely:-

$$(i) \quad P_1 = \frac{1}{10} \text{ atm}, \quad T_1 = 290^\circ\text{K}$$

$$(ii) \quad P_1 = \frac{1}{100} \text{ atm}, \quad T_1 = 290^\circ\text{K}.$$

The driving conditions needed to produce such strong shocks have been calculated assuming "ideal" hydrogen ( $\gamma = 1.41$ ) to be the driving gas.

In conclusion, the test conditions available through expanding the flow behind the shock are presented for an expansion ratio of 225 and the question of flight simulation is discussed.

---

\* Department of Aeronautics, Imperial College. This work was done whilst acting as vacation consultant at R.A.E. during July-August 1957.

LIST OF CONTENTS

	<u>Page</u>
1 Introduction	3
2 Details of calculation	3
2.1 Conditions behind the shock	3
2.2 Shock tube performance	4
2.3 Test conditions	4
3 Results and discussion	5
3.1 Real gas effects on flow conditions behind the shock	5
3.2 Shock tube performance	7
3.3 Conditions after expansion	7
4 Flight simulation at hypersonic speeds	8
4.1 Blunt bodies	9
4.2 Slender bodies	9
5 Conclusions	10
List of symbols	11
References	12

LIST OF ILLUSTRATIONS

	<u>Figure</u>
Flow temperatures	1a
Stagnation temperatures	1b
Pressure ratio across the shock	2
Density ratio across the shock	3
Velocity behind the shock	4
Mach numbers behind the shock	5
Stagnation pressure behind the shock	6
Stagnation conditions	7
Reynolds numbers per foot behind the shock	8
Effects of heating the driver gas	9
Shock-tube performance	10
Flow conditions after an expansion ratio of 225	11
Simulation near the nose of a blunt body	12

## 1 Introduction

For shock strengths  $M_s > 3$  real gas effects become increasingly important and for  $M_s > 6$ , perfect gas results are of little value. Calculations using real gas tables have been made by many authors, e.g. refs. 2, 3 (incorrect tables), 4, 5, 6 (corrected tables).

The corrected tables<sup>1</sup> permit calculation up to real gas temperatures of 15,000°K and Woods<sup>6</sup> has used these to calculate the R.A.E. shock tube performance up to a real gas temperature  $T_2$  of 8,000°K. In this note, the higher temperature conditions are examined. Any relaxation time effects have been neglected - i.e., the gas is assumed to be in the thermodynamic equilibrium and no attempt has been made to allow for shock attenuation.

## 2 Details of calculation\*

Two sets of initial conditions were chosen:-

$$(i) P_1 = \frac{1}{10} \text{ atm} = 1.47 \text{ p.s.i.} \quad T_1 = 290^\circ\text{K}$$

$$\rho_1 = 0.000235 \text{ slugs/cu ft} \quad H_1 = 3.124 \times 10^6 \text{ ft lb/slug}$$

$$(ii) P_1 = \frac{1}{100} \text{ atm} = 0.147 \text{ p.s.i.} \quad T_1 = 290^\circ\text{K}$$

$$\rho_1 = 0.0000235 \text{ slugs/cu ft} \quad H_1 = 3.124 \times 10^6 \text{ ft lb/slug.}$$

### 2.1 Conditions behind the shock

Conditions behind a normal shock were found by a method similar to that given by Bird<sup>3</sup>. The main difference arose in the treatment of the equation

$$H_2 - H_1 = \frac{1}{2} (P_2 - P_1) \left( \frac{1}{\rho_2} + \frac{1}{\rho_1} \right)$$

to obtain  $\rho_2$ . The presentation of the data in the new tables<sup>1</sup> made it more convenient to proceed as follows (than to follow the sequence described by Bird<sup>3</sup>):-

- (i) Given  $H_1$ ,  $P_1$  and  $\rho_1$ .
- (ii) Choose a value of  $T_2$ .
- (iii) Plot  $(H_2 - H_1)$  and  $\frac{1}{2} (P_2 - P_1) \left( \frac{1}{\rho_2} + \frac{1}{\rho_1} \right)$  against  $\rho_2$  from the tables<sup>1</sup>. The point of intersection of the two curves gives  $\rho_2$ .
- (iv) Read off the corresponding  $P_2$ ,  $H_2$  and  $S_2$  from the tables for the chosen  $T_2$ .
- (v) Repeat the process for other values of  $T_2$ .

---

\* See list of symbols for definitions, page 11.

$M_s$  and  $u_2$  were found from

$$M_s^2 = \frac{P_2 - P_1}{a_1^2 \rho_1^2 \left( \frac{1}{\rho_1} - \frac{1}{\rho_2} \right)}$$

derived from the momentum and energy equations, and

$$u_2 = a_1 M_s \left( 1 - \frac{\rho_1}{\rho_2} \right) \text{ continuity.}$$

The stagnation temperature and pressure (defined as those obtained by bringing the shock compressed air in region 2 isentropically to rest) were interpolated from the tables by calculating the stagnation enthalpy

$$H_{2_{st}} = H_2 + \frac{u_2^2}{2}$$

and moving along the isentrope  $S_2$  until this value was reached.

These calculations enabled conditions behind the shock to be plotted against shock Mach number  $M_s$  and the results are shown in Figs. 1 to 8 inclusive.

## 2.2 Shock tube performance

The shock tube performance was calculated for each set of initial conditions assuming the driver gas to be ideal hydrogen ( $\gamma_4 = 1.41$ ) at a pressure  $P_4$  of 1000 atmospheres and various temperatures  $T_4$  ranging from 290°K to 5,000°K. Again a graphical solution<sup>3</sup> was employed.  $P_2$  was plotted against  $u_2$  from the previous calculations (section 2.1).  $P_3$  was plotted against  $u_3$  on the same graph, using the unsteady isentropic expansion relations

$$\frac{a_4}{a_3} = \left( \frac{P_4}{P_3} \right)^{\frac{\gamma_4 - 1}{2\gamma_4}} = 1 + \frac{\gamma_4 - 1}{2} M_3^2$$

(see for example ref.7). The point of intersection of the two curves gives the shock tube solution  $P_2 = P_3$  and  $u_2 = u_3$ .

This enabled the shock strength that could be generated by each of two initial pressure ratios  $P_4/P_1$  to be plotted against driver temperature (Fig.9). A cross plot of  $P_4/P_1$  against  $M_s$  for a given  $T_4$  is presented in Fig.10. The additional real air values were calculated at  $M_3 = 1$  assuming that  $P_2/P_1$  is independent of  $P_1$  (see Fig.2).

## 2.3 Test conditions

The test section conditions in a non-reflected type of hypersonic shock tube with a nozzle expansion ratio of 225 were calculated assuming steady isentropic flow by solving the equations

$$\rho_2 u_2 A_2 = \rho_\infty u_\infty A_\infty \quad \text{where} \quad \frac{A_\infty}{A_2} = 225 \quad \text{- continuity} \quad (1)$$

$$H_2 + \frac{1}{2} u_2^2 = H_\infty + \frac{1}{2} u_\infty^2 = H_{2st} \quad \text{- energy} \quad (2)$$

$$S_2 = S_\infty \quad \text{- entropy} \quad (3)$$

Knowing all conditions 2, a  $T_\infty$  is selected so that  $\rho_\infty$  and  $H_\infty$  can be read off the tables at the given  $S$ . Velocity  $u_\infty$  is calculated from equation (2) and the product  $\rho_\infty u_\infty$  is plotted against  $T_\infty$ . This is repeated for a range of  $T_\infty$  and the value satisfying equation (1) picked off. The corresponding  $u_\infty$  and  $Z_\infty$  are interpolated from tables whilst  $\rho_\infty$  is calculated from equation (1).  $P_\infty$  follows from  $P = Z\rho RT$ .

The test conditions were plotted to a base of  $M_s$  (Fig.11).

### 3 Results and discussion

#### 3.1 Real gas effects on flow conditions behind the shock

The flow temperature  $T_2$  falls far below the ideal value (Fig.1a) for shock strengths  $M_s > 6$ . This is due to the large increases in specific heat or heat capacity caused by

- (a) excitation of vibrational modes
- (b) dissociation
- (c) excitation of electrons
- (d) ionisation.

The approximate temperature bands in which dissociation and ionisation occur are marked on the figure. Thus the flow temperature in the region of the stagnation point of a missile travelling with twenty times the speed of sound at 100,000 ft will be around 7,500°K instead of 24,000°K predicted by perfect gas theory.

The corresponding stagnation temperatures in region 2 are presented in Fig.1b.

Fig.2 gives the pressure ratio  $P_2/P_1$  across the shock, which closely follows the perfect gas law and is nearly independent of initial pressure  $P_1$ . From the shock wave equations,

$$\frac{P_2}{P_1} = a_1^2 \frac{\rho_1}{P_1} \left( 1 - \frac{\rho_1}{\rho_2} \right) M_s^2 + 1.$$

For strong shocks  $\rho_2 \gg \rho_1$ , so that  $\frac{P_2}{P_1} \approx a_1^2 \frac{\rho_1}{P_1} M_s^2$ , which for low temperatures  $T_1$  becomes  $\gamma M_s^2$  (see Fig.2). Hence real gas effects are expected to be small.

The drop in temperature  $T_2$  and only slight variation in pressure  $P_2$  imply an increased density in the real gas which is shown as the

density ratio  $\rho_2/\rho_1$  in Fig.3. The values are more than double the perfect gas estimates and the kinks correspond to dissociation and ionisation phenomena.

The velocity behind the shock,  $u_2$ , is similar for real and perfect gases as expected from the continuity equation

$$u_2 = a_1 M_s \left(1 - \frac{\rho_1}{\rho_2}\right) \simeq a_1 M_s \quad \text{for large } M_s.$$

This approximate relation is also marked on Fig.4.

The real gas Mach number  $M_2$  (Fig.5) rises to above 3 as compared with the perfect gas asymptote of 1.89 due to the reduced  $T_2$  decreasing the speed of sound  $a_2$ . The values of  $a_2$  (not given in the tables) have been calculated using ref.4 where  $a^2 = \gamma P/\rho$  and in that report  $\gamma$

is defined as 
$$\gamma = \left(\frac{\partial \log P}{\partial \log \rho}\right)_S.$$

The most striking real gas effect is on stagnation pressures assuming isentropic compression in the region behind the shock (Fig.6). For a shock Mach number of twenty, the real gas values are between ten and fifteen times the perfect values for the two cases considered. The reasons for the increase are (i) more energy is needed to produce a given  $M_s$  in real air than in a perfect gas - this can be seen from a comparison of the driving pressure ratios  $P_4/P_1$  (Fig.10); (ii) the larger density  $\rho_2$  in the real gas case.

These large stagnation pressures give an indication of the reservoir conditions needed to generate high temperature flows.

In Fig.7, the stagnation pressure ratio  $P_{2st}/P_1$  is plotted against stagnation temperature ratio  $T_{2st}/T_1$  for both the single shock followed by steady isentropic compression, and steady isentropic flow. Curves for real and perfect gases are shown. The perfect gas relations are

$$\frac{P_{2st}}{P_1} \rightarrow \left(1 + \frac{1}{\gamma_1}\right)^{\frac{1}{\gamma_1-1}} \left(\frac{\gamma_1+1}{\gamma_1-1}\right) \frac{T_{2st}}{T_1} = 23 \frac{T_{2st}}{T_1} \quad \begin{array}{l} \text{shock compression case} \\ \text{for large } M_s, \text{ putting} \\ \gamma_1 = 1.4 \end{array}$$

$$\text{and} \quad \frac{P_{2st}}{P_1} = \left(\frac{T_{2st}}{T_1}\right)^{\frac{\gamma_1}{\gamma_1-1}} = \left(\frac{T_{2st}}{T_1}\right)^{3.5} \quad \begin{array}{l} \text{for steady isentropic} \\ \text{flow.} \end{array}$$

Comparing the real gas curves, shock compression to the same stagnation pressure  $P_{2st}$  gives around three times the stagnation temperature that would be achieved isentropically. Conversely for a given  $T_{2st}$  the stagnation pressure achieved is only one thousandth of that obtained by steady isentropic compression.



Finally in Fig.8 the Reynolds number per foot obtainable in region 2 is plotted versus  $M_s$ . The shape of the curve reflects the density changes since plots of both  $u_2$  and  $\mu_2$  against  $M_s$  are sensibly smooth. The theoretical values for viscosity are taken from "Thermodynamics and Physics of Matter" by Rossini, p.374 Table D.6.b., and do not allow for the effects of dissociation.

### 3.2 Shock tube performance

The shock strengths that can be generated by perfect dry hydrogen at 1000 atmospheres and various temperatures are shown in Figs. 9 and 10 and compared with the perfect gas solutions<sup>7</sup>

$$\frac{P_4}{P_1} = \frac{P_2}{P_1} \cdot \frac{P_4}{P_3} = \left\{ \frac{2\gamma_1}{\gamma_1+1} M_s^2 - \frac{\gamma_1-1}{\gamma_1+1} \right\} \left\{ 1 - \frac{a_1}{a_4} \left( \frac{\gamma_4-1}{\gamma_1+1} \right) \left( M_s - \frac{1}{M_s} \right) \right\}^{\frac{-2\gamma_4}{\gamma_4-1}}$$

The benefit of heating the driver gas is marked; at pressure ratios above  $10^3$  the shock Mach number is roughly doubled by heating the hydrogen to 2000°K. For example, with dry hydrogen at  $P_4 = 1000$  atm and  $T_4 = 2000^\circ\text{K}$ , shock strengths rising to  $M_s = 26$  are possible in real air as the initial pressure  $P_1$  is reduced to  $10^{-2}$  atm.

Such a temperature can be attained by constant volume combustion of a hydrogen-oxygen mixture, but this results in a wet driver gas of increased molecular weight. The speed of sound  $a_4$  is thus reduced and this reduction decreases  $M_s$  by comparison with the values shown on Fig.10. These effects are more fully discussed in ref.6.

Heating by electrical discharge is also a possibility though there is little data on the behaviour of arcs at high pressures in hydrogen<sup>8</sup>.

### 3.3 Conditions after expansion

The working section conditions with a nozzle of area ratio 225 are presented in Fig.11. Although the test density, pressure and velocity are representative of high altitude hypersonic flight, the flow temperature and hence Mach number are not. This result is obvious from Fig.7, which shows how entirely different are the pressure-temperature relations for shock compression and isentropic expansion. With the low channel

pressures  $\left( P_1 = \frac{1}{10} \text{ and } \frac{1}{100} \text{ atm} \right)$  considered here, there are two possible sets of test conditions:

- (i) correct pressures, but high flow temperatures;
- (ii) correct temperatures, but very low pressures.

The second alternative requires extremely large nozzle expansion ratios and it will be difficult to avoid slip flow. The remedy is to use higher values of  $P_1$  or ideally, compression and expansion processes having similar pressure temperature relations. The conclusion is that for the conditions considered here, complete simulation is only possible at extreme altitudes.

#### 4 Flight simulation at hypersonic speeds

Consider hypersonic flight at 90,000 ft. The relevant atmospheric data<sup>14</sup> are  $P = 0.017$  atm,  $T = 218^\circ\text{K}$ ,  $\rho = 5.44 \times 10^{-5}$  slugs/cu ft and no dissociation or ionisation. Obviously, if a full scale model of all or part of a vehicle can be tested in a stream of undissociated air with the above flow conditions and at the correct velocity, then simulation is complete (the model would have to be preheated if equilibrium temperature conditions are needed, since the testing time is so short). Limiting the discussion to shock compression and isentropic expansion of real air the following table can be compiled:-

TEST MACH NO. $M_\infty$		5	10	15	20	
(1)	$(1 + 2M_\infty^2) 218^\circ\text{K}$	Perfect gas stagnation temp.	1,310	4,580	10,000	17,600
(2)	$T_{2st}$	Real gas stagnation temp. from Fig.1b - extrapolating for $P_1 = 1$ atm	1,310	4,300	6,700	9,500
(3)	$M_S$	Read off Fig.1b using row (1)	3.2	6.8	9.8	13
(4)	$\frac{T_{2st}}{T_1}$	$T_1 = 290^\circ\text{K}$	4.5	14.8	23.1	32.8
(5)	$\frac{P_{2st}}{P_1}$	From the shock compression curve of Fig.7. Extrapolate for $P_1 = 1$ atm	53	600	2,000	4,000
(6)	$\frac{P_{2st}}{P_\infty}$	From steady isentropic flow curve of Fig.7. Extrapolate for $P_1 = 1$ atm	250	$10^5$	of order $10^6$	of order $10^7$
(7)	$P_1$ required	$= \frac{(6)}{(5)} \times 0.017$ atm	0.8 atm	2.8 atm	of order 10 atm	of order 50 atm
(8)	$P_4$ required	From Fig.10 assuming $T_4 = 2,000^\circ\text{K}$	16 atm	400 atm	4,500 atm	70,000 atm
(9)	Expansion ratio	Taken from ref.2 approx, only	40	1,000	20,000	300,000

Strictly, the values for  $M_\infty = 10, 15$  and  $20$  need iteration for the correct  $P_1$  but the object is merely to indicate orders of magnitude. A similar calculation for simulation at an altitude of 180,000 ft showed a reduction of  $P_1$  and  $P_4$  by a factor 10. From these figures, it is obvious that if complete simulation at the higher Mach numbers is required then

- (i) the channel must be pressurised;
- (ii) driving pressures will be very large;
- (iii) extremely big expansions will be needed so that the testing of fairly large models is possible.

#### 4.1 Blunt bodies

For some investigations, Mach number is an unimportant parameter. Kurzweg and Wilson<sup>9</sup> show that for blunt bodies, the local Mach numbers around a major part of the nose region are independent of flight Mach numbers above 5. The important quantities are local density and temperature. Fig.12 shows the real and simulated conditions. If the relaxation distance is small compared with the stand off distance then the gases in both cases will be in thermal equilibrium and of similar chemistry. In particular at the stagnation point both  $M$  and  $Re$  are of less importance than the flow chemistry. Fay and Riddell<sup>10</sup> show that for a stagnation point boundary layer in thermal equilibrium the important quantities are stagnation enthalpy and density. These can readily be simulated in the shock tube without expanding the flow. If, however, the layer has not reached equilibrium, there can be scale effects which make complete simulation more difficult.

#### 4.2 Slender bodies

Slender body results should theoretically correlate on the parameter  $(M^3 \sqrt{C}) / \sqrt{Re_x}$  if the leading edge is sharp, but the experimental work of Bogdonoff and Hammitt<sup>11</sup> and the more recent theory of Lees<sup>12</sup>, have shown the extreme importance of the leading edge. In reality no edge is sharp and the body pressures seem to depend on the leading edge thickness and shock wave shape. It is possible to simulate conditions at the edge correctly and the shock wave shape alters very little at  $M_\infty > 10$ .

Moreover a considerable portion of the mass that enters the boundary layer has crossed a near normal detached shock at the leading edge and so may have the correct flow properties. What will certainly be wrong is the transverse temperature gradient between the edges of the boundary layer and the shock wave at stations well downstream from the nose, unless  $M_\infty$  is correctly simulated.

The various ways of using a shock tunnel showing simulated conditions and the corresponding difficulties are tabulated below.

The flow characteristics are

P,	$P_{st}$ ,	$\rho$ ,	$\rho_{st}$ ,	T,	$T_{st}$ ,	u,	M,	Re,	H
1	2	3	4	5	6	7	8	9	10

/Table

Type of Tube	Initial Conditions	Quantities Simulated	Difficulties
Basic tube plus large expansion to the correct $M_\infty$	$P_1 > 1$ atm	1-10 incl.	Lengthy nozzle; long starting time; very high $P_4$
Basic tube	Adjust for desired $4 + 10$	2,4,6,7,9,10. Flow at the stagnation point	Small model - could use a small expansion to avoid this
Basic tube plus expansion to $M_\infty = 5$	Vary $P_1$ for range of 9	2,4,6,7,9,10. Flow around the nose of blunt bodies	
Basic tube plus expansion to $M_\infty = 10$ or to correct value	Low $M_s$ $\therefore$ low $\frac{P_4}{P_1}$	1,3,8,9. No real gas effects	Dry air, operate just above air liquefaction temperature

## 5 Conclusions

- (i) For the conditions considered in this report the real gas effects on pressure and velocity behind the shock are small.
- (ii) The real gas effects on density, temperature, Mach number and particularly on stagnation pressure, are marked.
- (iii) For a hydrogen-driving-air shock tube the shock strength  $M_s$  is reduced by 5-10% at a given pressure ratio  $P_4/P_1$  due to real gas effects.
- (iv) There is a marked increase in the shock strength if the driver gas is heated.
- (v) Complete simulation of flight conditions in a shock tunnel is very difficult, basically because of the dissimilar compression and expansion cycles used to generate the flow, and a pressurised channel will usually be needed. Complete simulation of the flow near the stagnation point is however much simpler.

## Acknowledgment

This work was done at R.A.E. Farnborough whilst the author was engaged there under the Ministry of Supply Vacation Consultants Scheme during July and August 1957. The author wishes to extend his thanks to Mr. R. J. Monaghan and Mr. J. M. Shaw for their interest, guidance and constructive criticism, and to Fg.Off. B. Woods for many helpful suggestions.

LIST OF SYMBOLS

P	pressure
$\rho$	density
T	temperature
R	gas constant
u	flow velocity
U	shock velocity
S	specific entropy
H	specific enthalpy
$\gamma$	ratio of specific heats
a	local speed of sound
M	Mach number
Re	Reynolds number
C	constant in viscosity-temperature relation $\frac{\mu}{\mu_{\infty}} = C \frac{T}{T_{\infty}}$
$\mu$	viscosity
Z	compressibility factor ( $= 1 + \alpha$ where $\alpha$ is the fraction of the original number of molecules that has dissociated)
A	area

Subscripts

1	Conditions in front of shock wave
2	Conditions behind shock wave
3	Conditions behind interface
4	Conditions behind rarefaction fan, i.e. initial high pressure chamber conditions
s	shock wave
st	stagnation conditions
$\infty$	test conditions
x	distance from the leading edge

REFERENCES

- | <u>No.</u> | <u>Author</u>                           | <u>Title, etc</u>  |
|------------|---|--|
| 1          | J. Hilsenrath<br>C.W. Beckett           | Tables of thermodynamic properties of argon-free air to 15,000°K.<br>U.S.A. AEDC-TN-56-12. September 1956.   |
| 2          | W. Squire<br>A. Hertzberg<br>W.E. Smith | Real gas effects in a hypersonic shock tunnel.<br>U.S.A. AEDC-TN-55-14. March 1955.  |
| 3          | G.A. Bird                               | Some methods of evaluating imperfect gas effects in aerodynamic problems.<br>RAE Tech Note No. Aero 2488. January 1957.                                    |
| 4          | W.E. Moeckel                            | Oblique-shock relations at hypersonic speeds for air in chemical equilibrium.<br>NACA TN 3895. January 1957.   |
| 5          | M.F. Romig                              | The normal shock properties for air in dissociation equilibrium.<br>Journal of the Aeronautical Sciences. February 1956.                                   |
| 6          | B. Woods                                | The performance of the RAE 6 inch high pressure shock tube .<br>(To be published)  |
| 7          | J. Lukasiewicz                          | Shock tube theory and applications.<br>NAE Canada Report 15, also ARC 15,653.<br>January 1950.   |
| 8          | R.A. Dutton                             | The heating of the driver gas in a shock tube by means of an electrical discharge.<br>Unpublished.   |
| 9          | H.H. Kurzweg<br>R.E. Wilson             | Experimental hyperballistics.<br>Aeronautical Engineering Review, p.32.<br>December 1956.  |
| 10         | J.A. Fay<br>D.R. Riddell<br>N.H. Kemp   | Stagnation point heat transfer in dissociated air flow.<br>Jet Propulsion, p.672. June 1957.   |
| 11         | S.M. Bogdonoff<br>A.G. Hammitt          | Fluid dynamic effects at speeds from M = 11 to 15.<br>Journal of the Aeronautical Sciences, p.108.<br>February 1956.                                       |
| 12         | L. Lees                                 | Influence of the leading edge shock wave on the laminar boundary layer at hypersonic speeds.<br>Journal of the Aeronautical Sciences, p.594.<br>June 1956. |
| 13         | -                                       | Tables 3.3 and 3.8a,b of "The Handbook of Supersonic Aerodynamics", Vol.1.   |

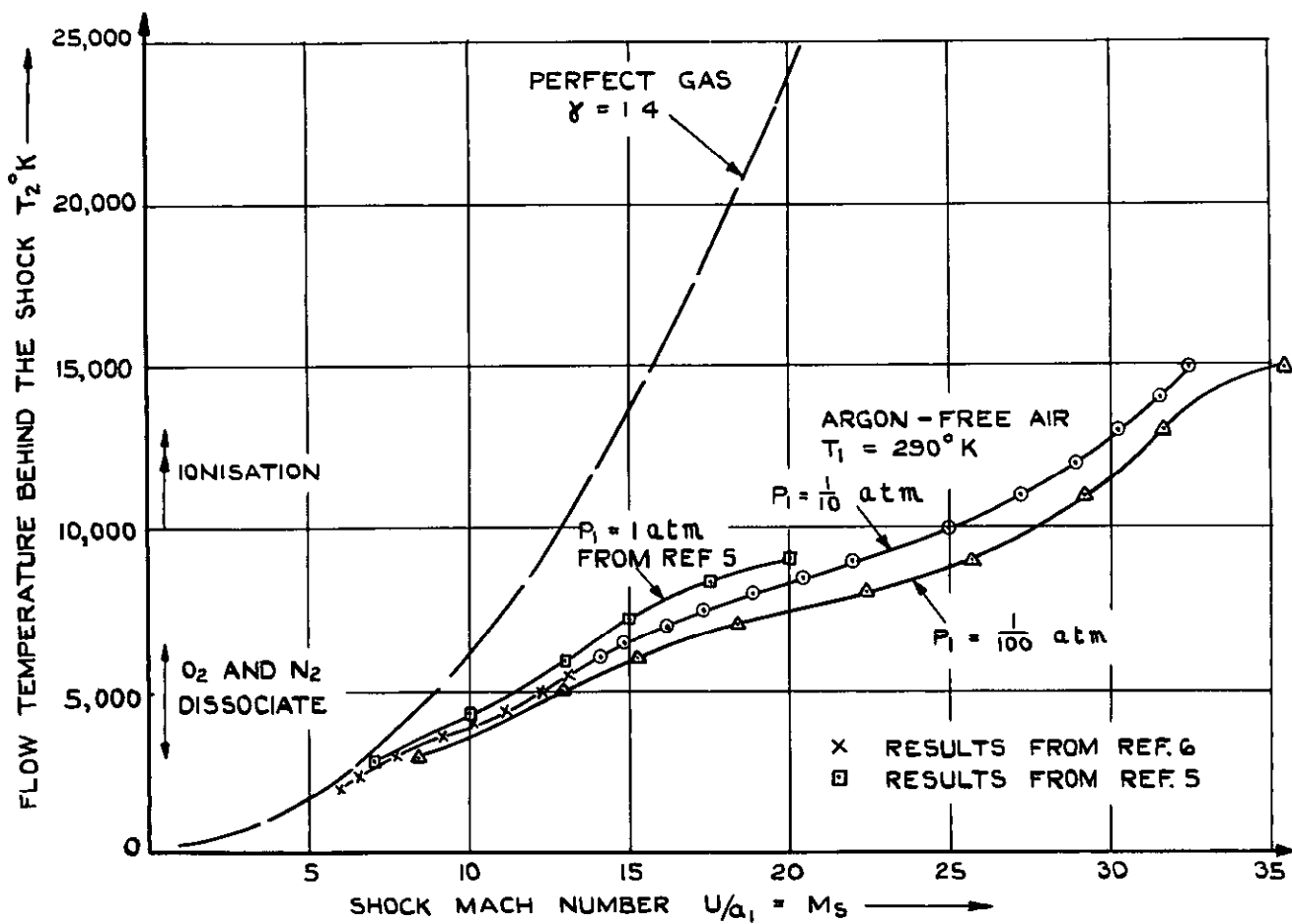


FIG. 1.(a) FLOW TEMPERATURES.

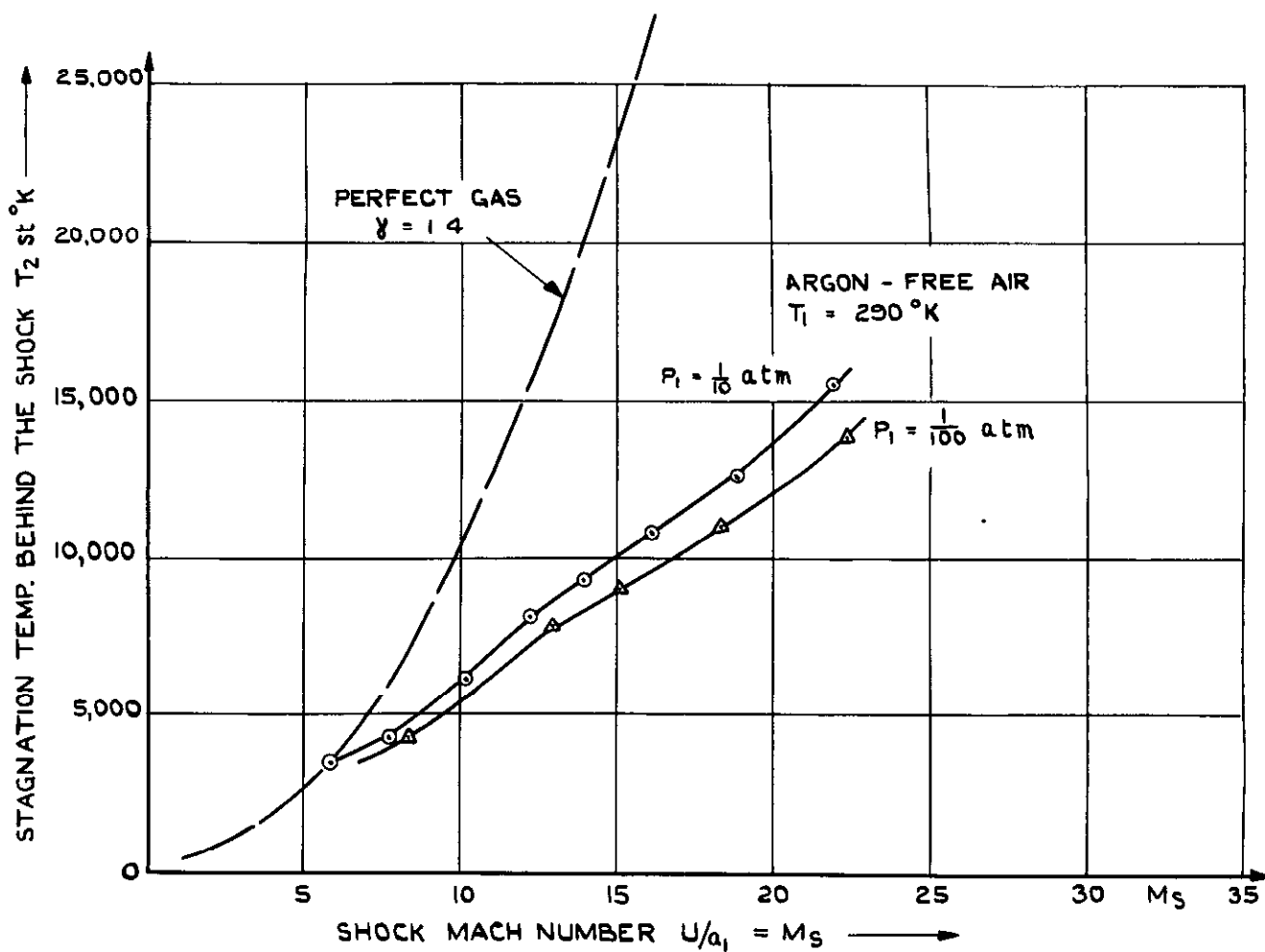


FIG. 1.(b) STAGNATION TEMPERATURES.

- X     $\odot$      $P_1 = \frac{1}{10}$  atm. (X ARE FROM REF 6.)
- $\Delta$      $P_1 = \frac{1}{100}$  atm
- APPROX. RELATION  $\frac{P_2}{P_1} = \gamma M_s^2$ .
- $\square$      $P_1 = 1\pi$  FROM REF. 5.

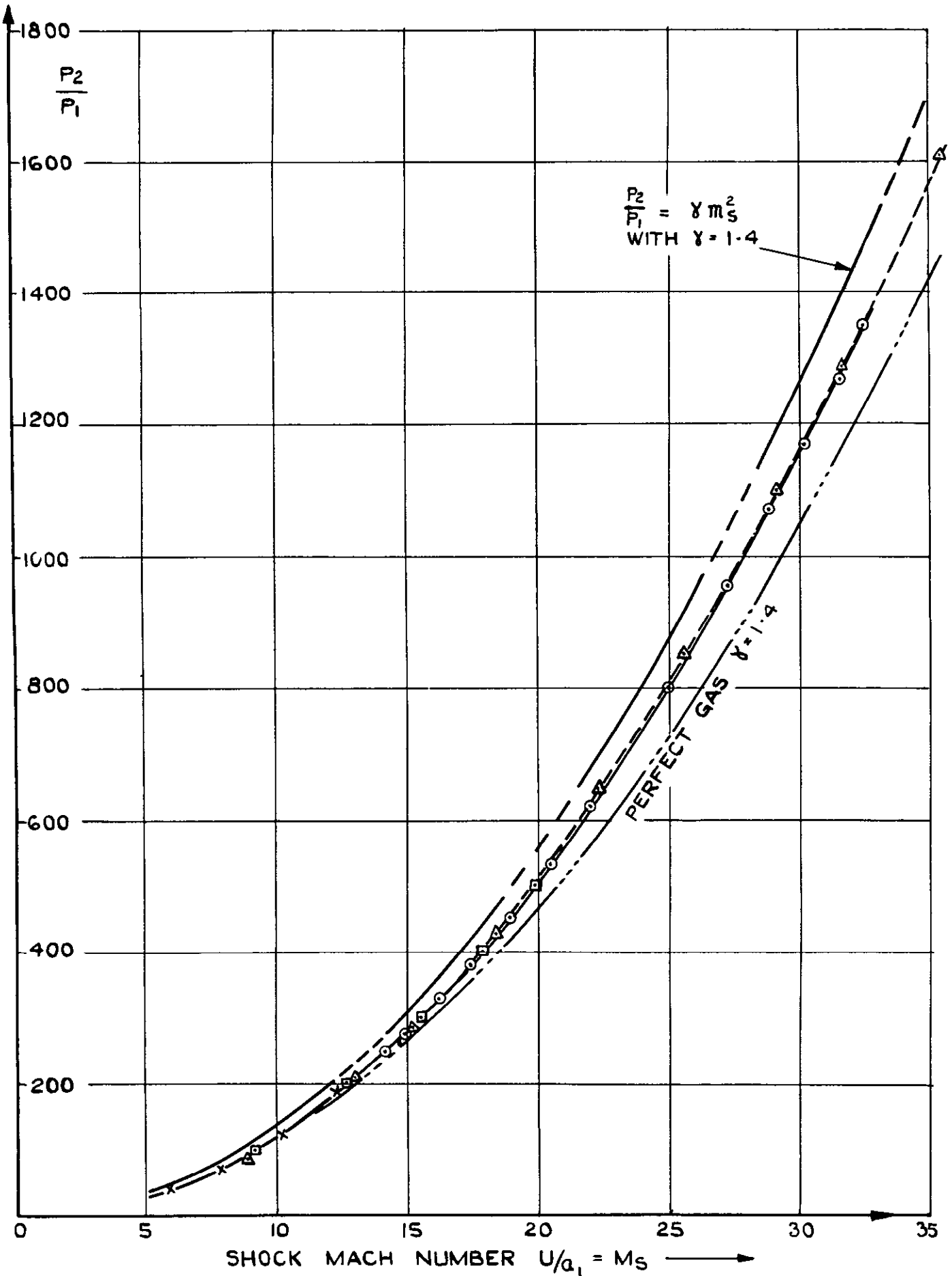


FIG. 2. PRESSURE RATIO ACROSS THE SHOCK.



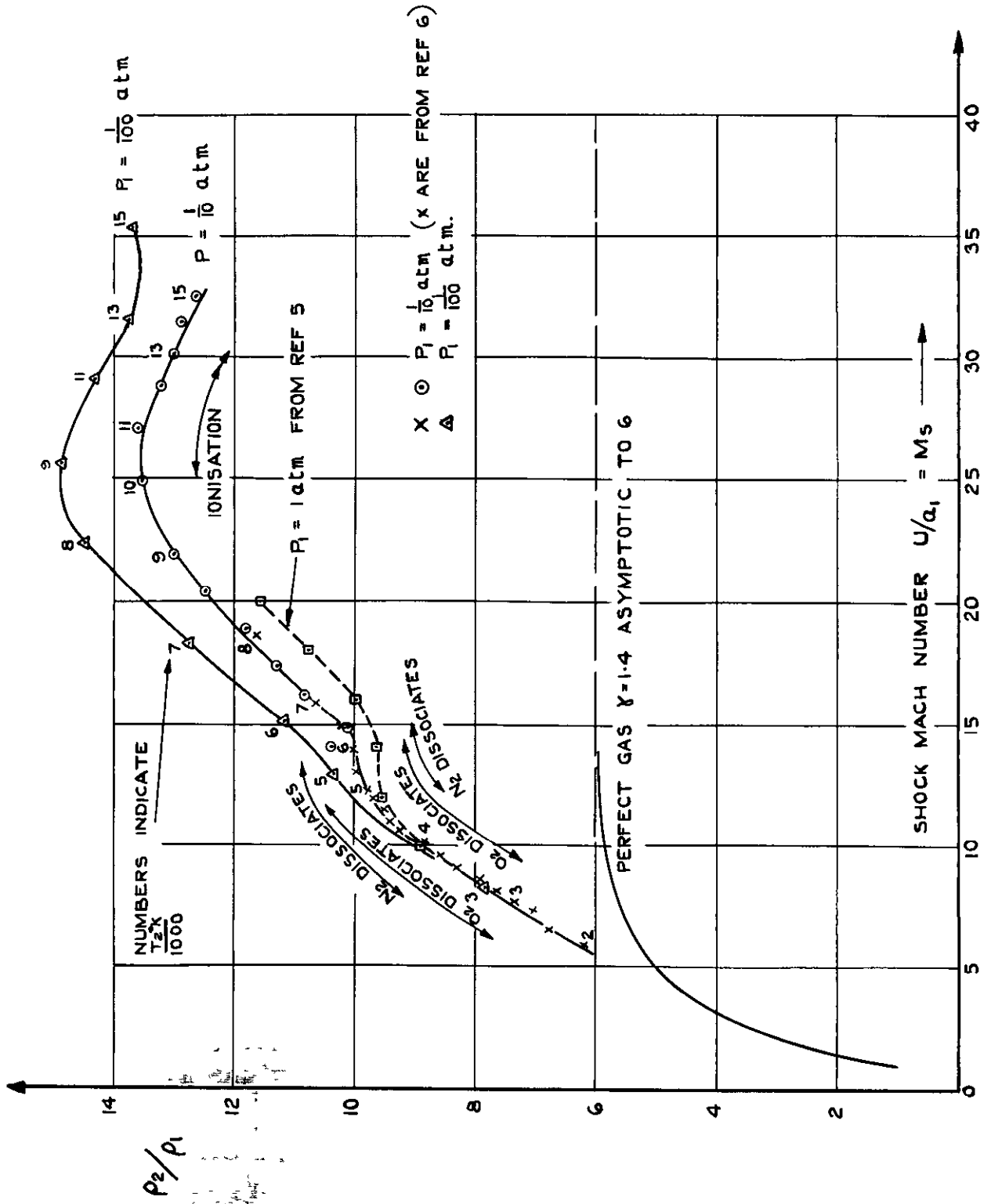


FIG. 3. DENSITY RATIO ACROSS THE SHOCK.

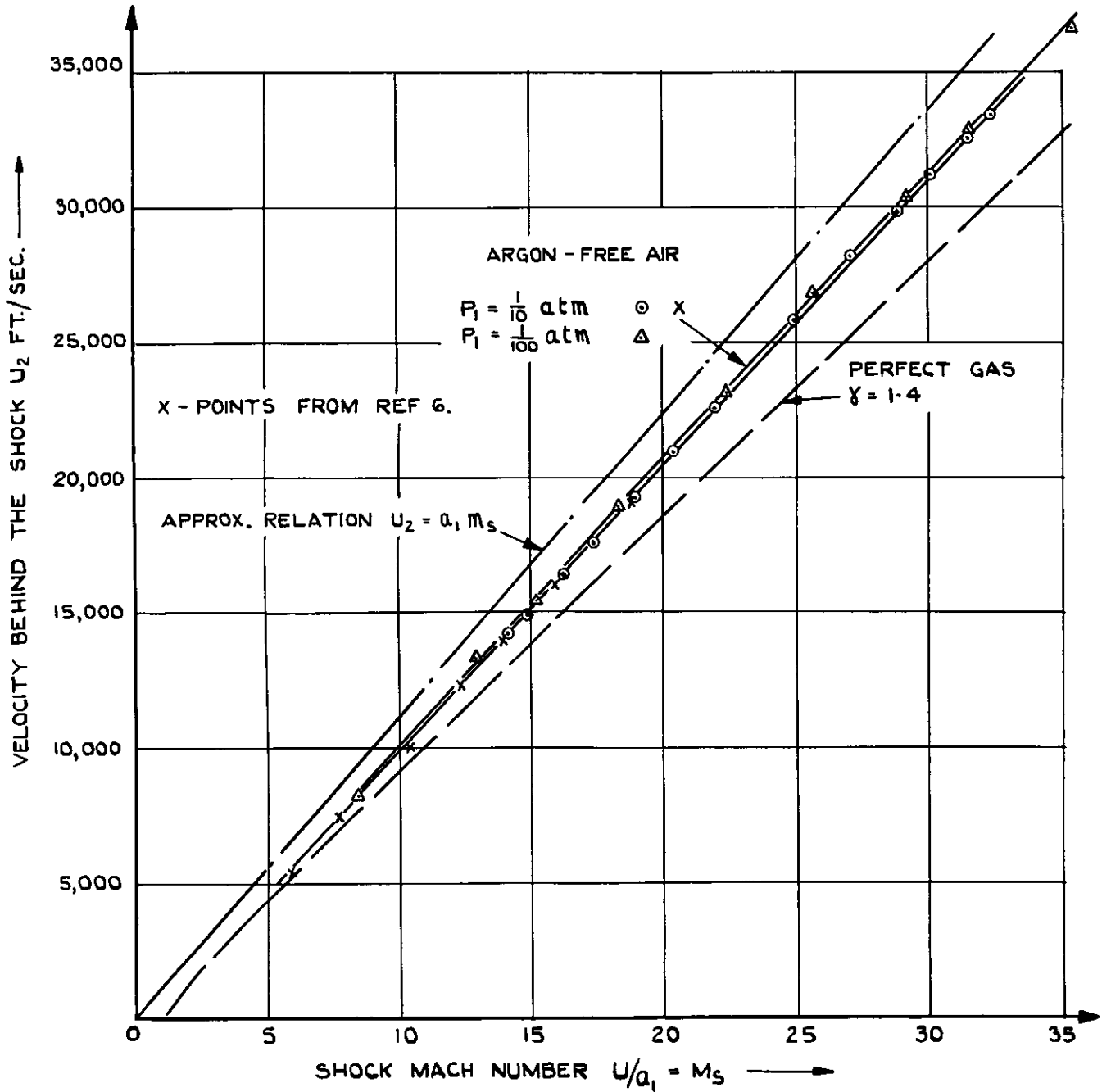


FIG. 4. VELOCITY BEHIND THE SHOCK.

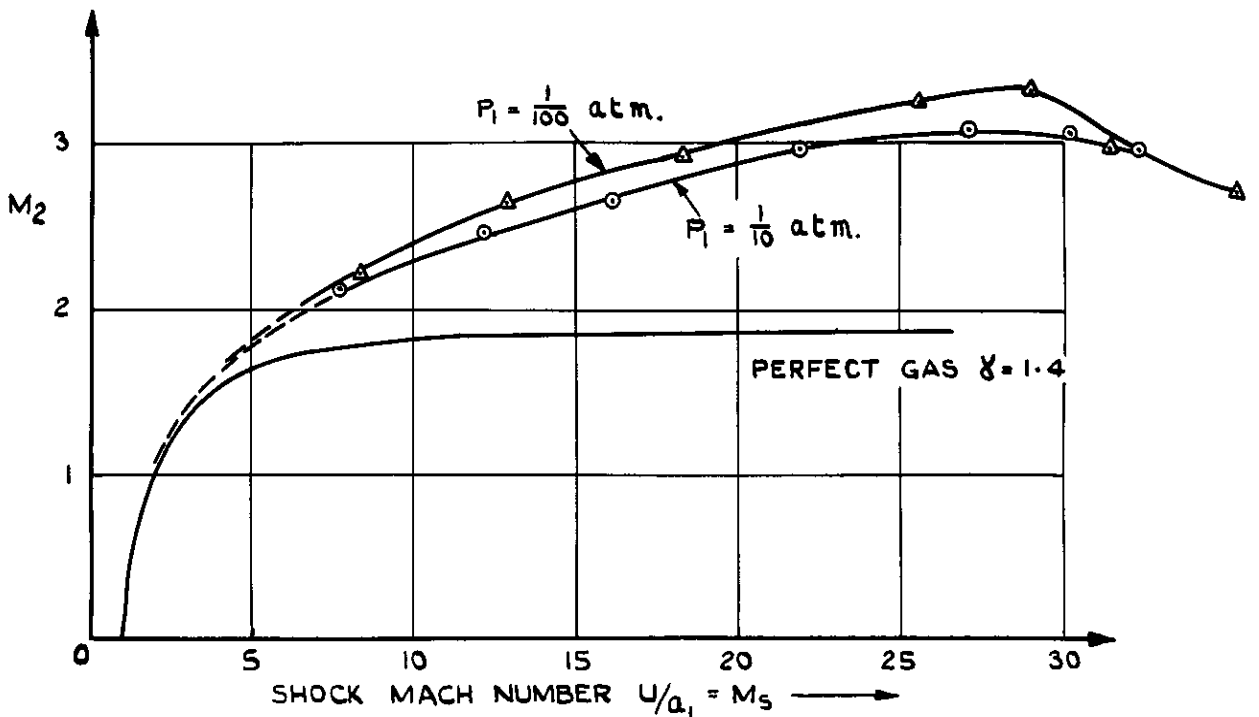
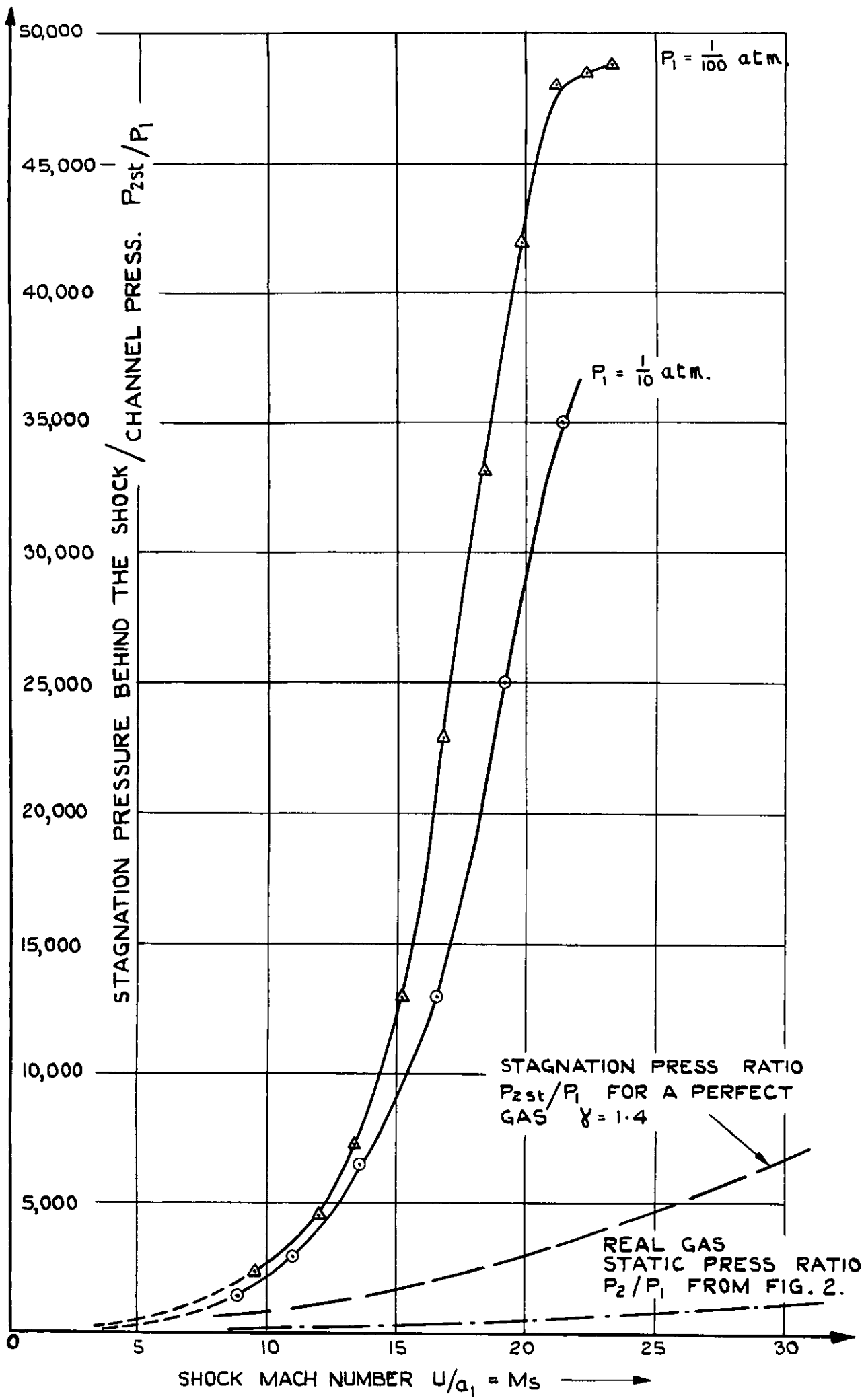


FIG. 5. MACH NUMBER BEHIND THE SHOCK.



**FIG. 6. STAGNATION PRESSURE BEHIND THE SHOCK.**

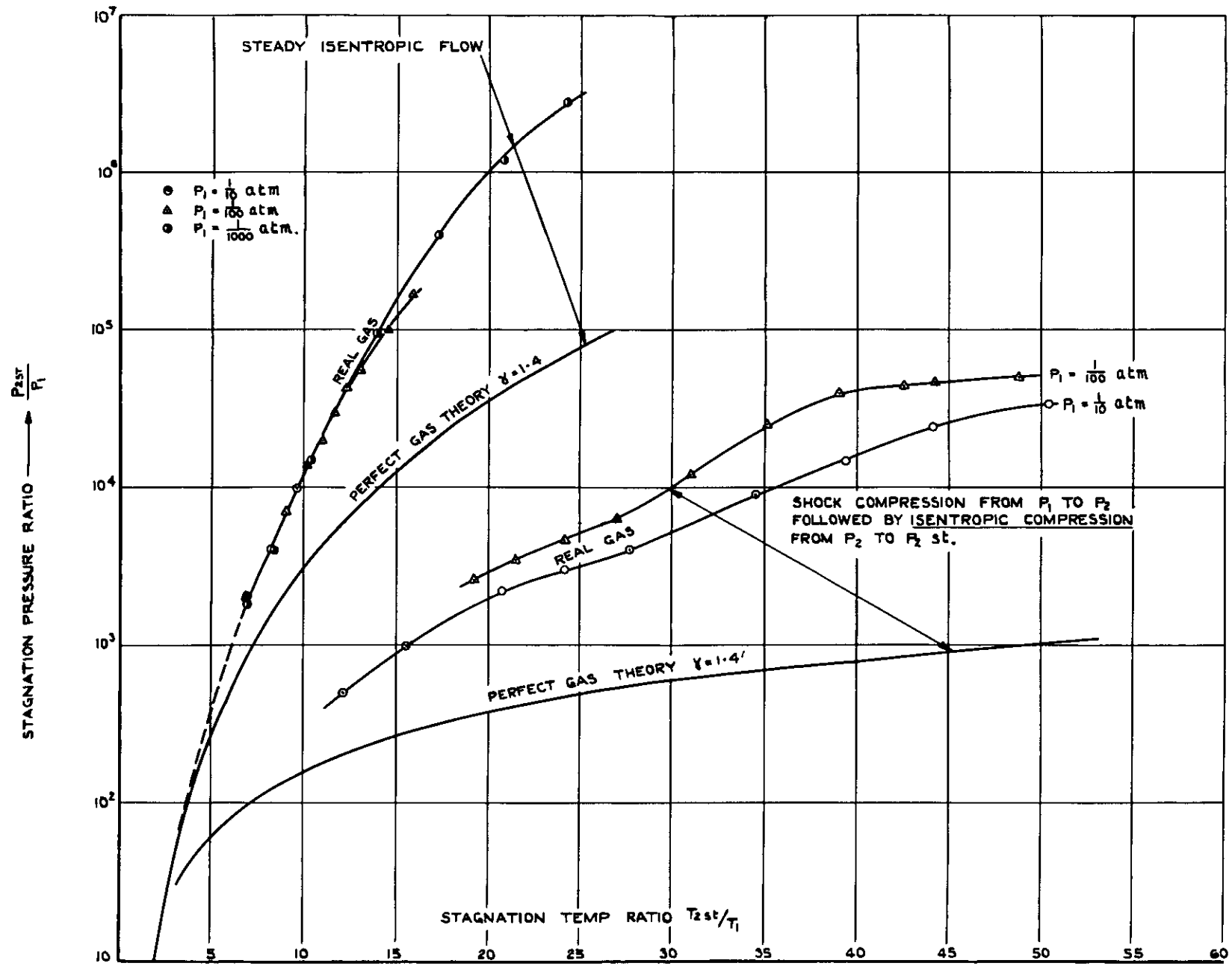


FIG. 7. STAGNATION CONDITIONS.

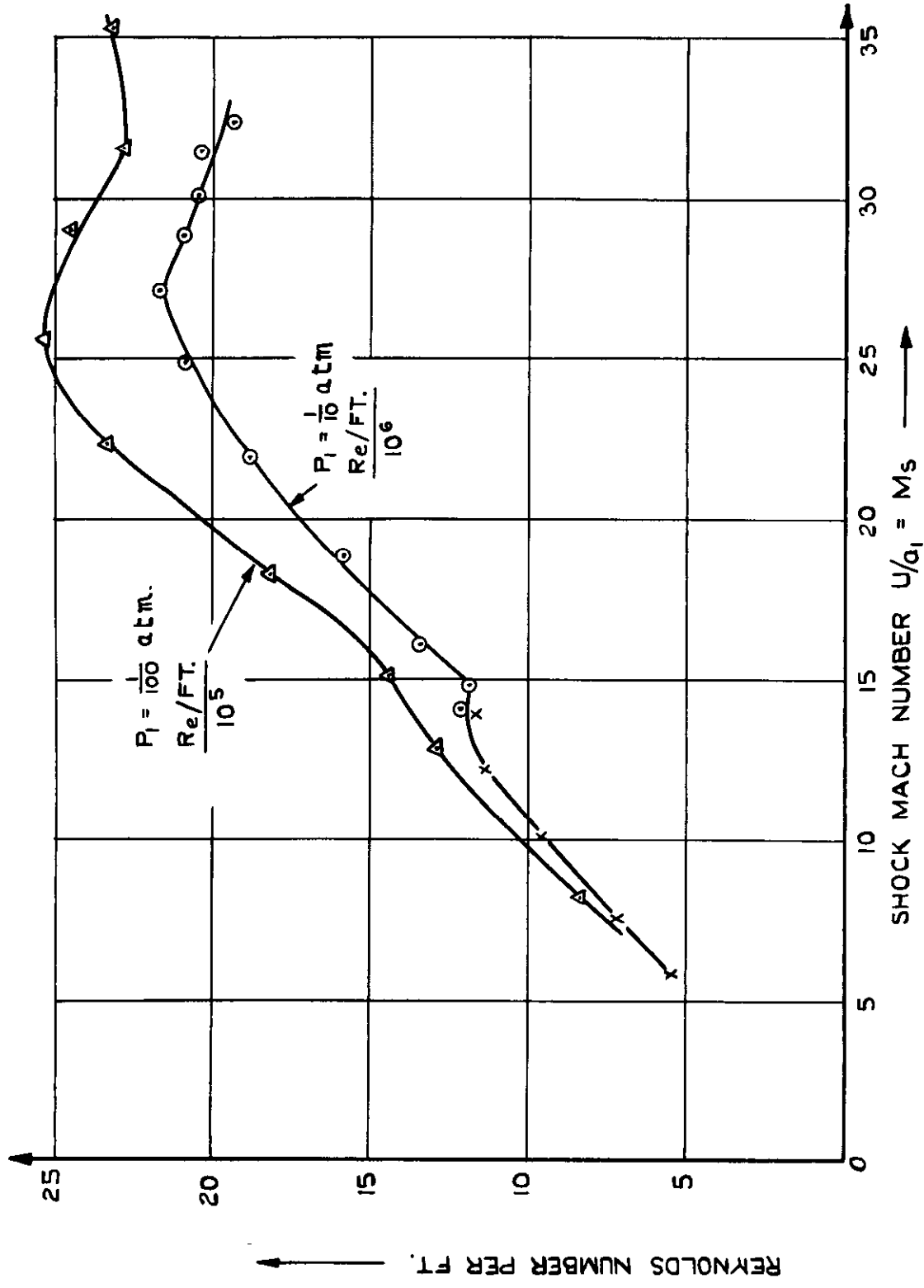


FIG. 8. REYNOLDS NUMBER PER FOOT BEHIND THE SHOCK.

DRIVER GAS IS PERFECT DRY H<sub>2</sub> ( $\gamma = 1.41$ ) AT  $P_4 = 1000$  ATM.  
 DRIVEN GAS IS REAL ARGON-FREE AIR AT  $T_1 = 290^\circ\text{K}$  AND VARIOUS  $P_1$

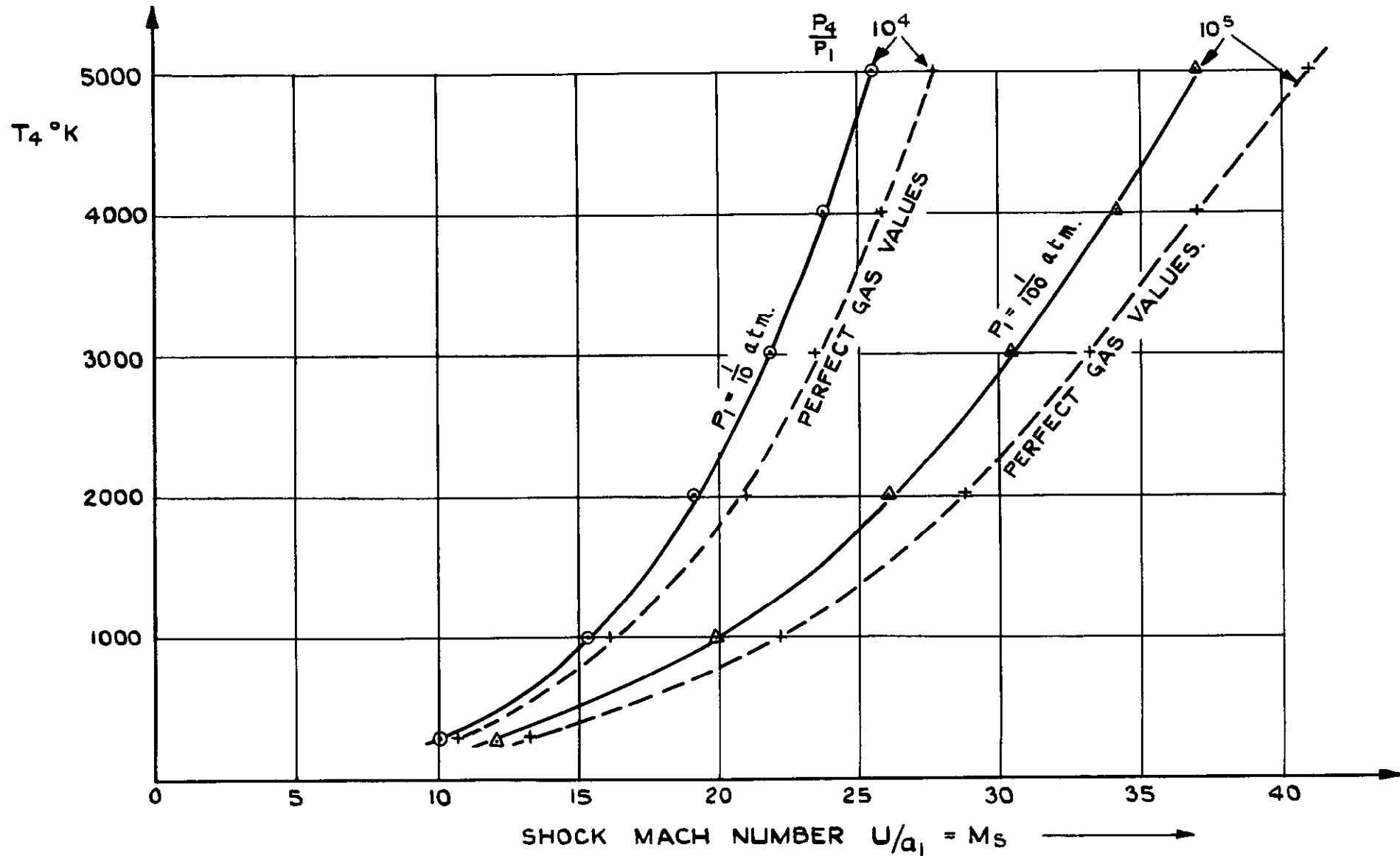


FIG. 9. EFFECTS OF HEATING THE DRIVER GAS.

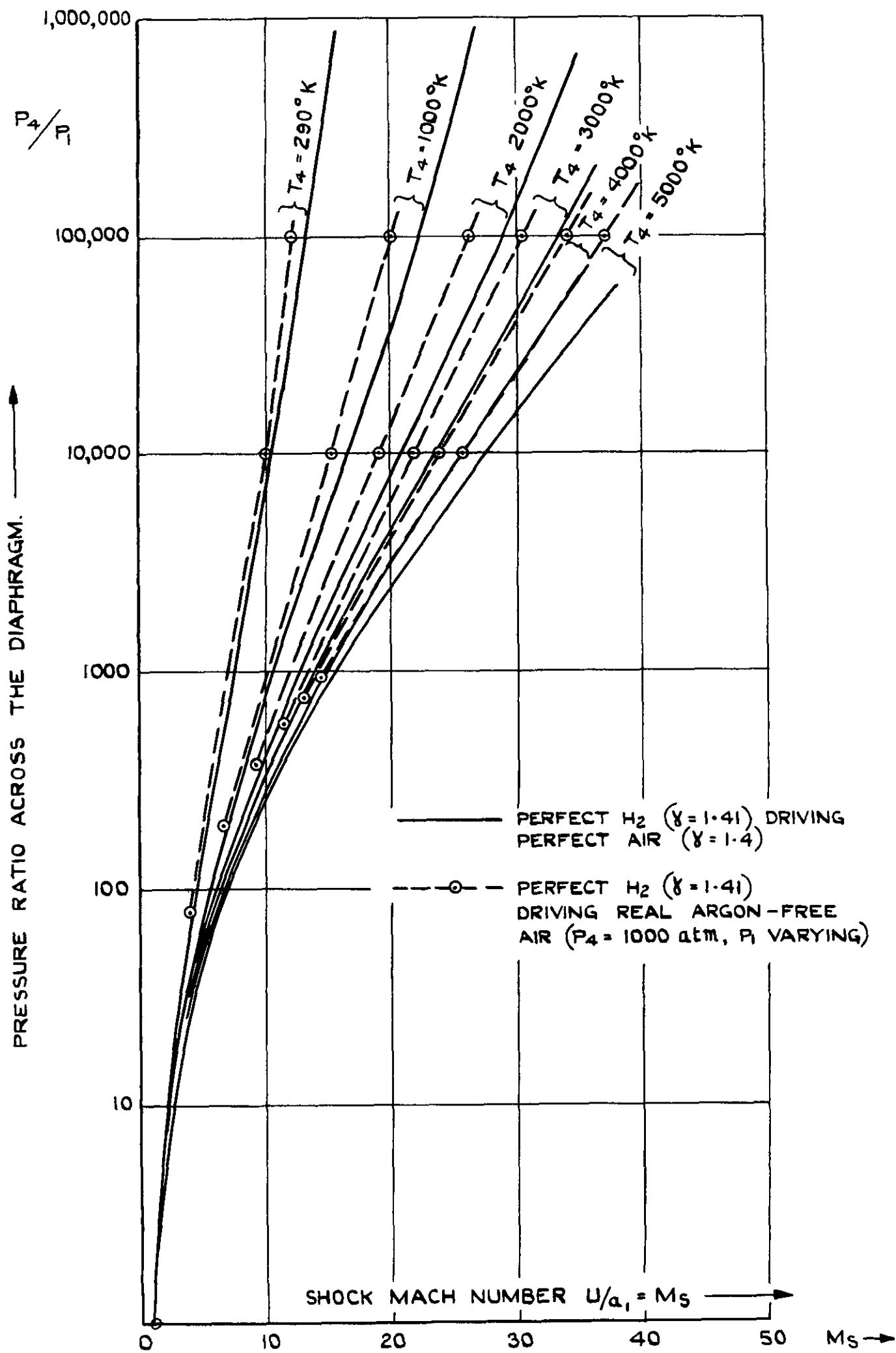


FIG. 10. SHOCK-TUBE PERFORMANCE.

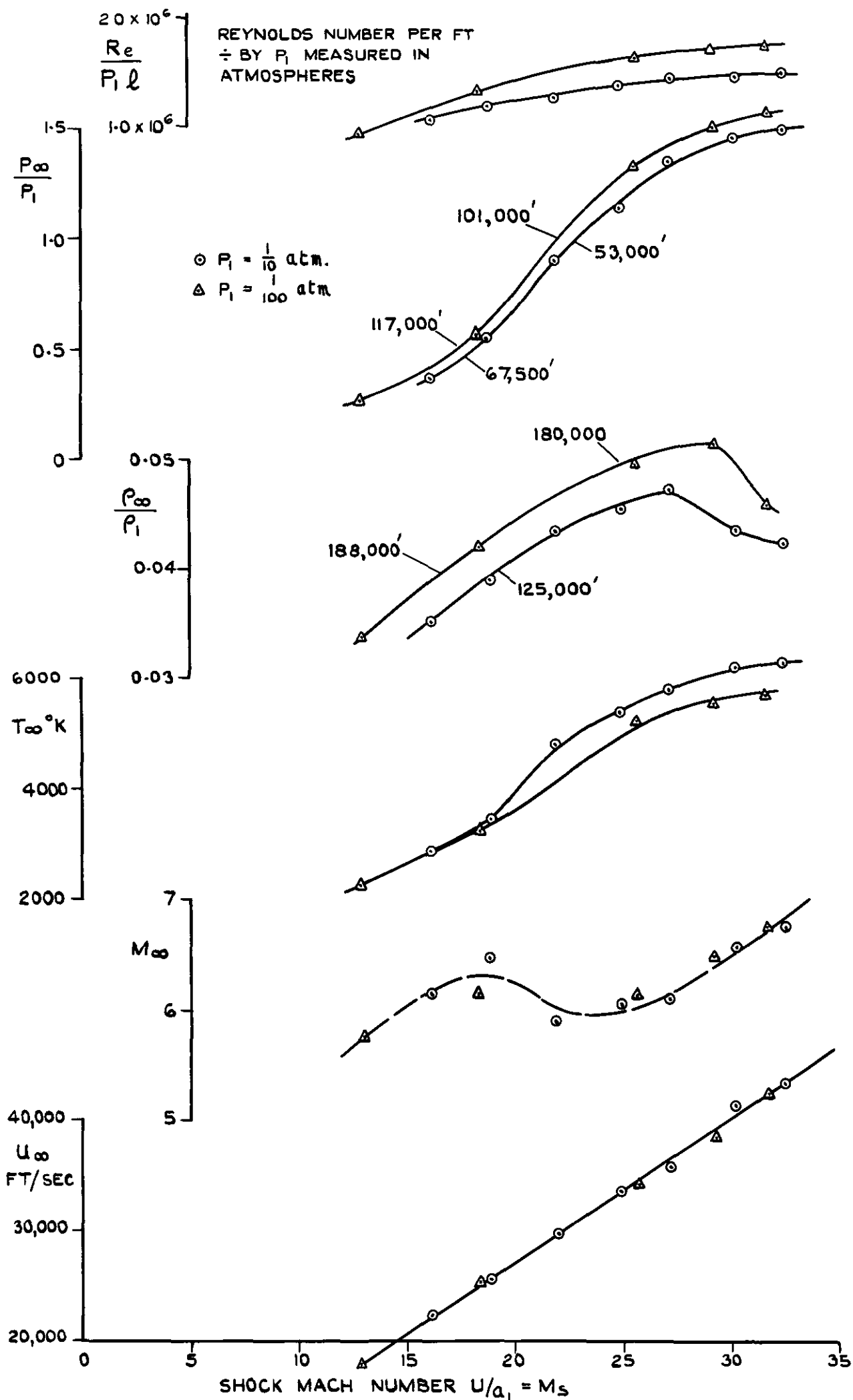
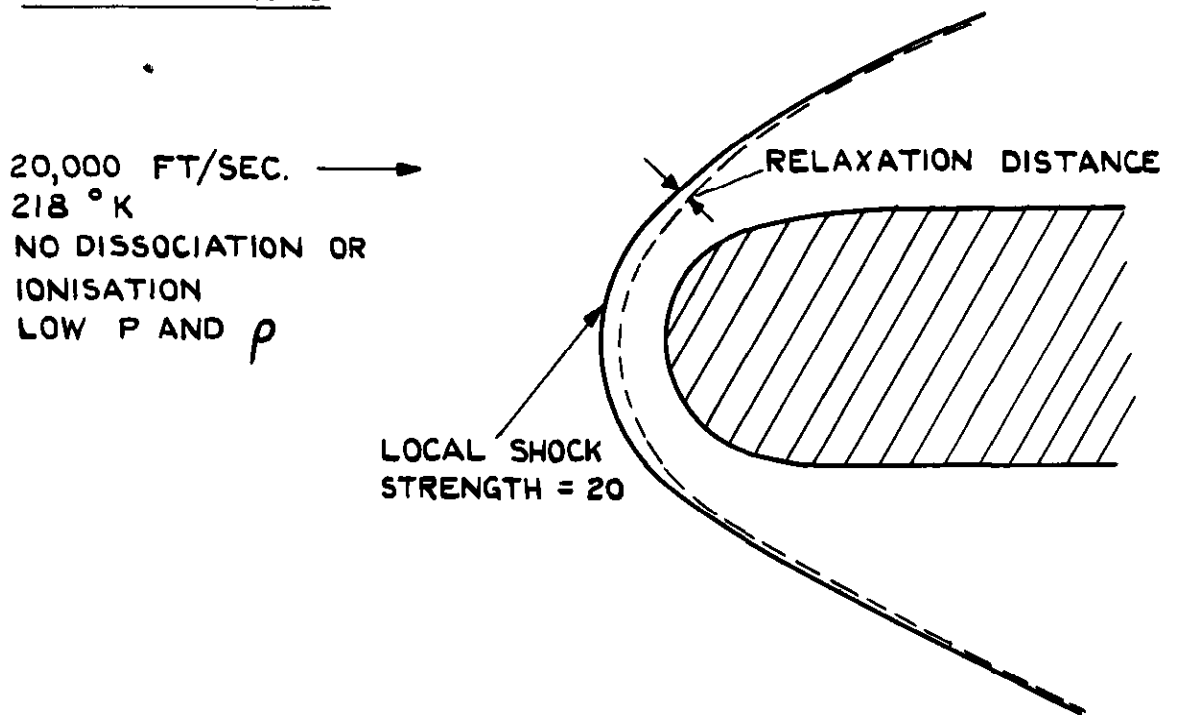


FIG. II. FLOW CONDITIONS AFTER AN EXPANSION RATIO OF 225.



REAL CONDITIONS.



SIMULATED CONDITIONS.

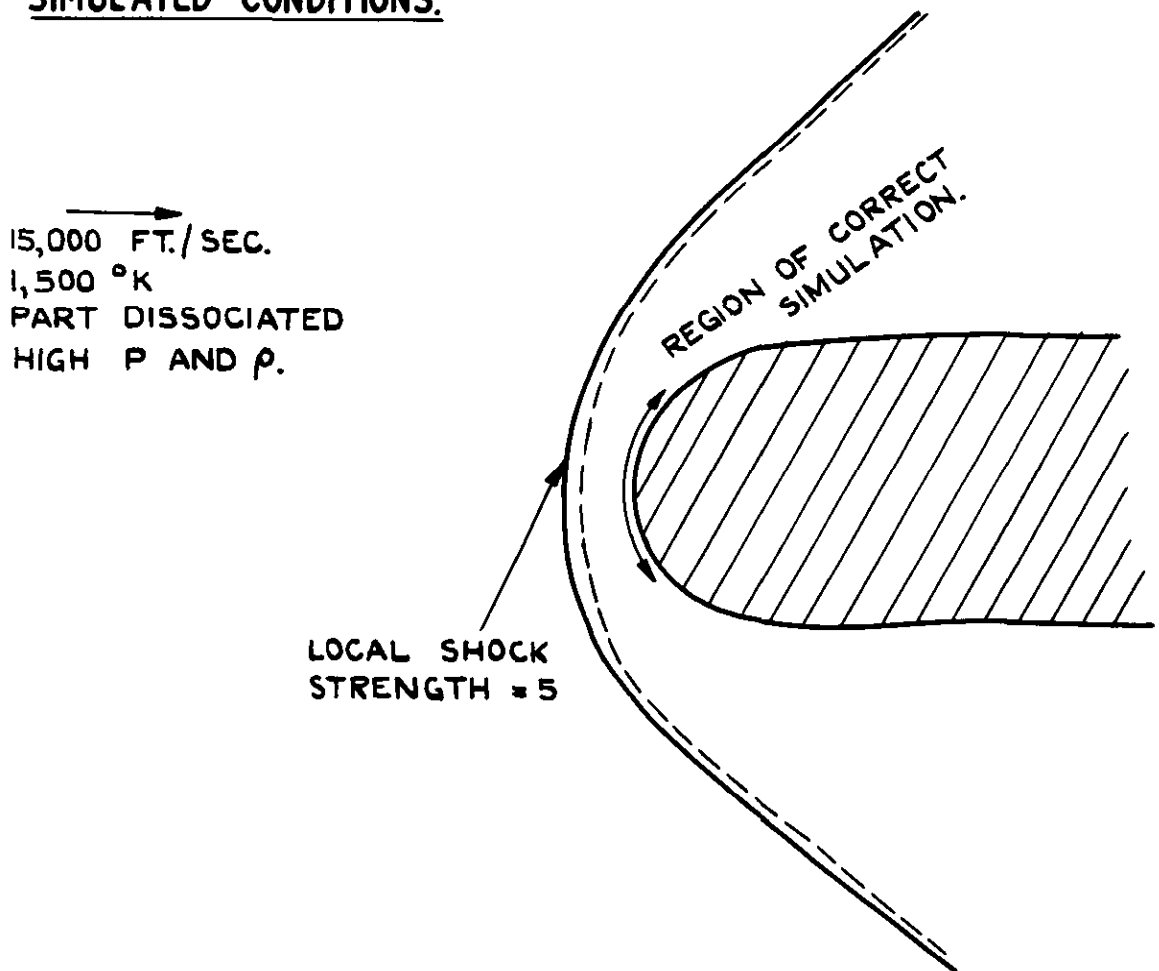


FIG. 12. SIMULATION NEAR THE NOSE  
OF A BLUNT BODY.

•

•

•

•

•

•

•

•



© *Crown copyright* 1958

Published by  
**HER MAJESTY'S STATIONERY OFFICE**

To be purchased from  
York House, Kingsway, London w c 2  
423 Oxford Street, London w.1  
13A Castle Street, Edinburgh 2  
109 St. Mary Street, Cardiff  
39 King Street, Manchester 2  
Tower Lane, Bristol 1  
2 Edmund Street, Birmingham 3  
80 Chichester Street, Belfast  
or through any bookseller

**PRINTED IN GREAT BRITAIN**